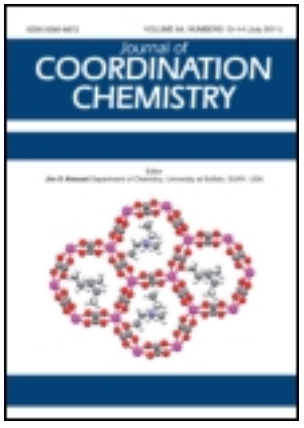

Journal of Coordination Chemistry
Publication details, including instructions for authors and subscription information:
http://www.tandfonline.com/loi/gcoo20

Structure, dynamics, and solvation in a disordered metal-organic coordination polymer: a multiscale study

Craig C. Jolley [a b], Janice Lucon [a], Masaki Uchida [a], Courtney Reichhardt [a c], Mary J. Vaughn [a], Ben J. Lafrance [a] & Trevor Douglas [a]

[a] Department of Chemistry & Biochemistry, Center for Bio-Inspired Nanomaterials, Montana State University, Bozeman, MT, USA

[b] Laboratory for Systems Biology, RIKEN Center for Developmental Biology, Kobe, Japan

[c] Department of Chemistry, Stanford University, Stanford, CA, USA

Published online: 29 Nov 2011.

To cite this article: Craig C. Jolley, Janice Lucon, Masaki Uchida, Courtney Reichhardt, Mary J. Vaughn, Ben J. Lafrance & Trevor Douglas (2011) Structure, dynamics, and solvation in a disordered metal-organic coordination polymer: a multiscale study, Journal of Coordination Chemistry, 64:24, 4301-4317, DOI: 10.1080/00958972.2011.637555

To link to this article: http://dx.doi.org/10.1080/00958972.2011.637555

Journal of Coordination Chemistry
Vol. 64, No. 24, 20 December 2011, 4301–4317

Structure, dynamics, and solvation in a disordered metal–organic coordination polymer: a multiscale study

CRAIG C. JOLLEY*†‡, JANICE LUCON†, MASAKI UCHIDA†, COURTNEY REICHHARDT†§, MARY J. VAUGHN†, BEN J. LAFRANCE† and TREVOR DOUGLAS*†

†Department of Chemistry & Biochemistry, Center for Bio-Inspired Nanomaterials, Montana State University, Bozeman, MT, USA
‡Laboratory for Systems Biology, RIKEN Center for Developmental Biology, Kobe, Japan
§Department of Chemistry, Stanford University, Stanford, CA, USA

(*Received 7 September 2011; in final form 14 October 2011*)

Metal–organic coordination polymers are a growing class of technologically-important materials in which transition metal ions are connected by multitopic organic chelators to form a 3-D network structure. While the structures of many highly-ordered metal–organic frameworks have been determined, far less structural information is available about the more common disordered materials. Our study combines pair distribution function analysis from total X-ray scattering, *ab initio* quantum mechanical calculations, and all-atom molecular dynamics to explore the structure and dynamics of a poorly-ordered branched coordination polymer. The polymer structure is highly flexible and dynamic, and is dramatically affected by its solvation state, a finding with far-reaching implications for the incorporation of coordination polymers into nanocomposite materials.

Keywords: Coordination polymer; Molecular dynamics; Quantum chemistry

1. Introduction

One of the most daunting challenges in modern materials science is the development of truly rational approaches to the synthesis of new materials with desired functional properties. It has been observed [1] that the synthesis of traditional materials is more of an art than a science – reactants combine to form a bulk material through the formation of covalent bonds, often undergoing dramatic changes in the process. The lack of structural correlation between reactants and products makes prediction (and therefore control) extremely difficult. To better control the structure of synthesized materials, it might be advantageous to combine stable building blocks which are joined together by weaker but specific supramolecular interactions. This is precisely the approach employed by biology, where highly specific interactions between ''prefabricated'' macromolecular components leads to the formation of heterogeneous, hierarchically

*Corresponding authors. Email: craig@cdb.riken.jp; tdouglas@chemistry.montana.edu

ISSN 0095-8972 print/ISSN 1029-0389 online © 2011 Taylor & Francis
http://dx.doi.org/10.1080/00958972.2011.637555

structured materials on a scale ranging from protein complexes to tissues and even organisms themselves.

One synthetic approach to the formation of supramolecular materials has emerged from the burgeoning field of metal–organic frameworks (MOFs) [1–4]. MOF synthesis typically begins with a solution of metal–chelating organic linkers, to which transition metal ions are added. The components assemble, often spontaneously and under rather mild conditions, to form 3-D networks of organic struts connecting metal–ion vertices. Considerable ingenuity has been employed to develop ion/ligand combinations that will assemble into well-ordered lattice structures, and MOFs are promising materials for applications in gas storage, drug delivery, catalysis, and sensor devices.

While regular lattice structures are desirable for some applications and certainly simplify the process of structure determination, crystallinity is not necessary for other applications and may interfere with more important design objectives. For example, a recent study [5] describes an optically healable supramolecular polymer consisting of rubbery poly(ethylene-*co*-butylene) domains linked together by 2,6-*bis*(1′-methylbenzimidazolyl)pyridine chelators coordinating Zn^{2+} ions – in this case the elastic properties of the material depend upon the disorder in the rubbery phase. Alternatively, functional design constraints on the organic linkers (e.g. requiring efficient electron transfer between metal centers) could be incompatible with the rather stringent demands of macroscopic order. Another recent report [6] describes the synthesis of a metal–organic branched coordination polymer inside a multimeric protein cage – this confined geometry is likely to interfere with the formation of macroscopic crystalline domains [7], even in materials that might assume more order in unconstrained environments. Fully harnessing the potential of disordered metal–organic coordination polymers will require methods of structural prediction and experimental validation based on the structure of the building blocks used in the synthesis.

Our study focuses on a simple class of coordination polymers formed by the reaction of 1,3-di-1,10-phenanthrolin-5-ylthiourea (bi-phen) (figure 1) with a series of transition metal ions – Fe^{2+}, Co^{2+}, Ni^{2+}, and Zn^{2+}. The system was chosen because the bi-phen linker has proven to be more effective in our aqueous coordination polymer synthesis than other ditopic ligands, allowing us to direct material formation through strong metal–ligand interactions. In addition, coordination polymers incorporating metal–phenanthroline complexes are an attractive target for photocatalytic and light-harvesting applications [8, 9]. Structural information about this material was obtained by pair distribution function (PDF) analysis from total X-ray scattering, a method that yields largely short-range information and says relatively little about the large-scale structure. Correct interpretation of PDF data typically requires an atomic-scale structural model, which was obtained through molecular modeling of the metal–organic coordination polymers using a molecular dynamics forcefield that was parameterized based on quantum-chemical studies of the polymer components. In addition to matching the data obtained in the PDF studies, the coordination polymer simulations yielded a wealth of additional information about the polymer structure and dynamics in both solvated and desolvated states. Due (in part) to the high charge density of the coordination polymer, solvation plays a crucial role in determining the structure and dynamics of the material. Careful selection of the solvent environment will be critical to any technological applications using similar materials. The approach outlined here

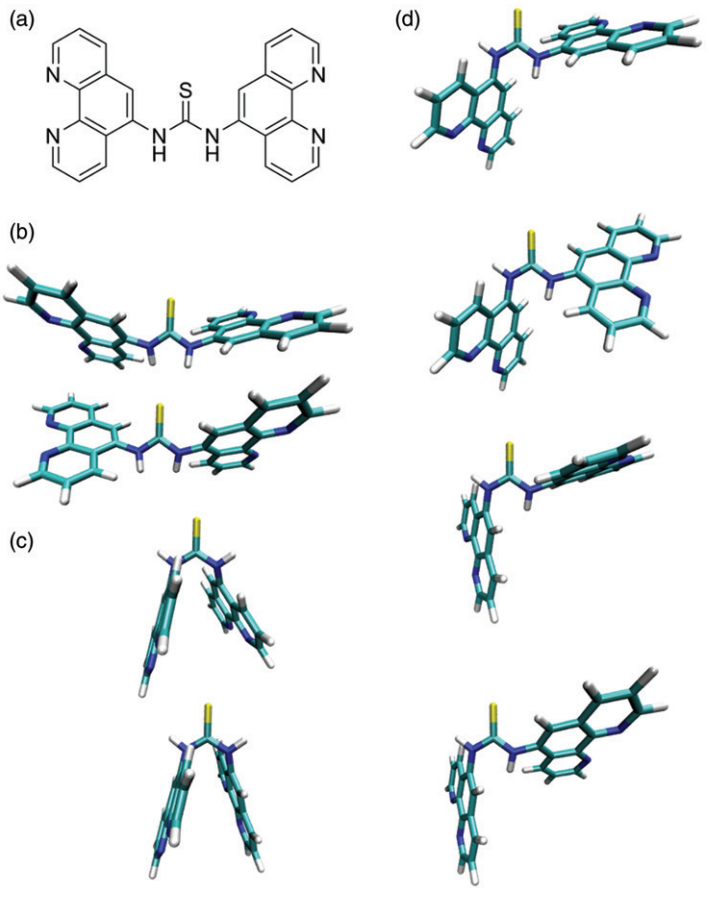

Figure 1. Structure of 1,3-di-1,10-phenanthrolin-5-ylthiourea (bi-phen) (a). By rotating about non-aromatic bonds, the linker can adopt eight different low-energy conformations; two extended (b), two contracted (c), and four *trans* (d).

should be broadly applicable to a range of metal–linker combinations, allowing computational prediction of the properties of these soft, amorphous materials.

2. Materials and methods

2.1. *Materials*

5-Amino-1,10-phenanthroline was purchased from Rubipy Scientific Inc. (Ottawa, Canada). All other starting materials were purchased from Sigma-Aldrich (St. Louis, MO) or Fisher Scientific (Waltham, MA). The THF was distilled over metallic sodium and benzophenone prior to use. All water used was purified using a MilliQ water system. All chemicals were used without purification, unless otherwise stated.

2.1. *1,3-Di-1,10-phenanthrolin-5-ylthiourea (bi-phen) synthesis*

The bi-phen linker was made *in situ* through the application of a procedure previously described for the formation of isothiocyanates [10]. A 50 mL round-bottomed flask was charged with 5-amino-1,10-phenanthroline (488 mg, 2.5 mmol), THF (10 mL), and sodium hydride (91 mg, 3.8 mmol). The flask was set in an ice bath under Ar atmosphere and the chemicals were stirred and mixed thoroughly. Carbon disulfide (480 μL, 8 mmol) was slowly injected *via* a syringe pump over 1 h as the reaction was brought up to room temperature. The mixture was then refluxed at 70°C for 20 h while maintaining an Ar atmosphere. The reaction was cooled on an ice bath followed by the addition of *p*-toluenesulfonyl chloride (524 mg, 2.75 mmol) and triethylamine (760 μL, 5.5 mmol) and was subsequently stirred for 3 h at room temperature. Dichloromethane (15 mL) and 1N hydrochloric acid were added to the reaction flask. The water layer was then washed twice with 10 mL of dichloromethane to remove residual reactants. The organic layer was discarded, while the water layer was stored at 4°C overnight, resulting in a pale orange precipitate which was isolated on a glass filter, washed with diethyl ether, and dried in a desiccator. The product was characterized by NMR and LC/MS. ^{1}H NMR: (500 MHz, DMSO-d_6) δ (ppm) 9.30 (d.d., $J_1 = 5$ Hz, $J_2 = 35$ Hz, 4H), 9.19 (d.d., $J_1 = 6.5$ Hz, $J_2 = 44.5$ Hz4H), 8.63 (s, 2H) and 8.27–8.22 (m, 4H). ^{13}C NMR: (500 MHz, DMSO-d_6) δ (ppm) 183.7, 148.9, 142.4, 138.8, 136.7. 136.5, 135.0, 129.2, 127.5, 125.6, 125.5, 123.7. LC/MS: M + H 433.124 (found), M + H 433.123 (Calcd).

2.3. *Coordination polymer synthesis*

The coordination polymers were all made following the same procedure. The metal ion sources were either zinc(II) nitrate hydrate, colbalt(II) nitrate hydrate, nickel(II) acetate, or ammonium Fe(II) sulfate hydrate. In a standard reaction, a flask was charged with a solution of bi-phen (21.4 mL, 0.214 mmole, 10 mmol L^{-1}, ethanol) followed by the addition of 1.43 mL of aqueous metal solution (100 mM) made immediately prior to addition. The resulting mixture was sonicated for 5 min and was subsequently heated at reflux for 4 h. Using a rotary evaporator, the reaction solvents were removed and the resulting solid was resuspended in 10 mL water, flash frozen in liquid nitrogen, and lyophilized (Labconco). The resulting powder was used without further purification. Aqueous suspensions of a portion of each solid were made with brief sonication. These suspensions were analyzed by dynamic light scattering, revealing that the material formed was supramolecular, exhibiting average hydrodynamic radii of 1300 nm (Zn), 440 nm (Co), 2100 nm (Ni), and 500 nm (Fe).

2.4. *PDF data collection*

Structural characterization of amorphous or nanocrystalline materials by total X-ray scattering and PDF analysis has been extensively described elsewhere [11, 12]. Briefly, the coordination polymer (and metal-free bi-phen) samples were dried to powder in a vacuum lyophilizer (Labconco) and packed into Kapton capillaries with an inner diameter of 0.0575″. X-ray scattering was collected on the beamline 11-ID-B of the Advanced Photon Source at Argonne National Laboratories, with an X-ray wavelength of 0.2128 Å. Powder diffraction patterns were collected using a Perkin-Elmer

amorphous Si area detector and assembled by averaging 5 s exposures, with a total exposure time of 5 min for each data set. Longer collection times (up to 1000 exposures) were attempted, but did not show noticeable improvements in the quality of the final PDF. Diffraction image data were processed using the Fit2D software package [13] and integrated to obtain a 1-D trace of the total scattering. The radial PDF $G(r)$ was then obtained *via* a Fourier transform of the corrected X-ray structure factor $S(Q)$; both $S(Q)$ and $G(r)$ were calculated using the PDFGetX2 software package [14] with a $Q_{\max}$ of 19.2 Å^{-1}.

2.5. *DFT calculations*

Minimized structures and normal modes were determined for the bi-phen linker as well as for the *tris*-phenanthroline complexes of Fe^{2+}, Co^{2+}, Ni^{2+}, Zn^{2+}, and Ru^{2+}. Although no experimental PDF data were obtained for polymers containing Ru^{2+}, it was included in the parameterization because of the potential utility of Ru-phenanthroline complexes in light-harvesting applications [8, 9]. The metal–phenanthroline calculations used density functional theory (DFT) implemented in the NWChem software package [15] with a B3LYP functional [16–19], 6-31G* basis sets for C, N, and H, and a LANL2DZ basis set [20–22] with an effective core potential for the central metal ion. Calculations for the smaller thiourea–phenanthroline linker used a B3LYP functional with 6-311++G** basis sets on C, N, and H, and a 6-311++G(2d,2p) basis set on S. Atomic partial charges were estimated using the electrostatic potential module in NWChem. While the metal–phenanthroline complexes are fairly rigid and yielded a single conformation, the bi-phen linker exhibits eight different local minima (figure 1), corresponding to $\sim 180^\circ$ rotations about the thiourea C–N bond and the bond from the thiourea N to the phenanthroline ring system. Although the normal mode frequencies returned by the DFT calculations were reasonable, they were not verified using vibrational spectroscopy. In future work, if force fields of this kind are to be used extensively for coordination polymer materials (especially in a predictive context), vibrational spectroscopy could provide a valuable check on the accuracy of the calculated normal mode frequencies.

2.6. *MM forcefield parameterization*

The DFT results were used to parameterize a classical molecular mechanics (MM) forcefield with the following form:

$$\begin{aligned} U(r) = & \sum_{\text{bonds}} k_b(b-b_0)^2 + \sum_{\text{angles}} \left(k_\theta(\theta-\theta_0)^2 + k_{\text{UB}}(r-r_0)^2\right) \\ & + \sum_{\text{dihedrals}} k_\chi(1+\cos(n\chi+\varphi)) \\ & + \sum_i \sum_j \left(-E_{ij}\left(\left(\frac{r_{\min}}{r_{ij}}\right)^{12} - 2\left(\frac{r_{\min}}{r_{ij}}\right)^{6}\right) - \varepsilon\frac{Cq_iq_j}{\varepsilon_0 r_{ij}}\right). \end{aligned}$$

Equilibrium values of the bond lengths (b_0), bond angles (θ_0), and second-nearest-neighbor distances (r_0) were obtained from the optimized geometries yielded by the

DFT calculations; equilibrium values of the dihedral angles were all assumed to be $\chi_0 = 180^\circ$ with a multiplicity of $n = 2$, based on the ideal planar geometry of the phenanthroline ring systems and the bi-phen linker. Partial charges q_i were obtained from electrostatic potential fitting of the DFT results, and VdW parameters ($E_{ij}, r_{\min}$) were assumed to be identical to the parameters for chemically-similar atoms in the standard CHARMM27 protein forcefield [23]. In particular, aromatic carbon (CA) and hydrogen (HP) and the unprotonated imidazole nitrogen in histidine (NR2) were used for the phenanthroline rings, the parameters for polar hydrogen (H), carbonyl carbon (C), amide nitrogen (NH2), and the cysteine/methionine sulfur (S) were used for thiourea, and the parameters for heme iron (FE) were used for all metal ions.

Appropriate spring constants for the bond, angle, Urey-Bradley, and dihedral terms (k_b, k_θ, k_{UB}, and k_χ) were determined by matching the MM normal modes calculated using CHARMM [24] with the DFT normal modes obtained using NWChem. The agreement between a set of quantum-mechanical normal modes $\{\mathbf{v}_i^{\mathrm{QM}}\}$ and a set of classical normal modes $\{\mathbf{v}_i^{\mathrm{C}}\}$ with frequencies $\{\upsilon_i^{\mathrm{QM}}\}$ and $\{\upsilon_i^{\mathrm{C}}\}$ can be quantified [25] as

$$Y^2 = \sum_{3N-6} \frac{\left(\nu_i^{\mathrm{QM}} - \nu_j^{\mathrm{C}}\right)^2}{\left|\mathbf{v}_i^{\mathrm{QM}} \cdot \mathbf{v}_j^{\mathrm{C}}\right|}.$$

For a given DFT mode $\mathbf{v}_i^{\mathrm{QM}}$, $\mathbf{v}_j^{\mathrm{C}}$ is the classical mode with the largest-magnitude dot product. For a given set of classical normal modes $\{\mathbf{v}_i^{\mathrm{C}}\}$, Y^2 can be decreased by either decreasing the difference between the mode classical and quantum frequencies, or making the atomic displacement vectors more similar (i.e., increasing the dot products in the denominator). An initial set of parameters was estimated by analogy with the CHARMM27 protein forcefield, and the mode agreement Y^2 was then optimized using a Metropolis Monte Carlo scheme. At each step, a randomly-selected spring constant parameter was multiplied by a uniform random number in $[1 - s/2, 1 + s/2]$, where s is the (adjustable) scale of random changes to the parameters. Changes were then accepted or rejected using the Metropolis criterion with an "energy scale" E; parameter changes that decreased Y^2 were always accepted, while changes increasing Y^2 were accepted with probability $e^{-\Delta Y^2/E}$.

An optimal parameter set was sought using a simulated annealing procedure in which E was decreased if the acceptance rate (averaged over the preceding 1000 steps) increased above 0.6 or a new minimum of Y^2 had not been reached in more than 1000 steps; s was decreased if the acceptance rate decreased below 0.4. In this way, the acceptance rate was maintained in a reasonable regime while both E and s decreased steadily over the course of the simulation, leading eventually to an optimized parameter set.

In some cases, the procedure exhibited overfitting – a set of parameters was found that gave a low value of Y^2 but contained physically-unrealistic values that led to instability when molecules were simulated at finite temperature using molecular dynamics. The problem was avoided by adding a restraint term to the overlap score:

$$Y^2 = \sum_{3N-6} \frac{\left(\nu_i^{\mathrm{QM}} - \nu_j^{\mathrm{C}}\right)^2}{\left|\mathbf{v}_i^{\mathrm{QM}} \cdot \mathbf{v}_j^{\mathrm{C}}\right|} + k \sum_{\text{parameters}} (p - p_{\text{initial}})^2,$$

where k is a tunable parameter that was decreased to zero during the course of the optimization, as it became clear that the system was settling into a physically-reasonable minimum. Typically, this restraint term made only a small contribution to Y^2; even a gentle restraint was sufficient to prevent overfitting.

In the case of the metal–phenanthroline complexes, Y^2 was calculated at each step for all five of the metals used ($Fe^{2+}, Ni^{2+}, Co^{2+}, Zn^{2+}$, and Ru^{2+}), leading to a set of parameters that was simultaneously optimized to a variety of different metals. As a result, the bonds internal to phenanthroline were fairly generic to different metal coordination situations. The interactions involving metal ions were, of course, specific to one of the five ions. During iterations in which one of these parameters was chosen, E was temporarily rescaled by 1/5 to account for the fact that only one of the five roughly equal contributions to Y^2 would be affected by such a move, leading to a smaller value for ΔY^2.

Once the parameters for the metal–phenanthroline complexes had been fully optimized, parameters were simultaneously optimized for the eight bi-phen conformations using a similar averaging scheme. Parameters that had already been optimized (i.e., those involved in the phenanthroline ring system) were held fixed during this round of optimization; essentially only the central thiourea moiety and the thiourea–phenanthroline connections were optimized at this stage. Because thiourea is not particularly similar to anything in the CHARMM27 protein forcefield, an optimization was first run on thiourea alone which, due to its small size, converged quickly to a reasonable parameter set. The thiourea parameters were then used as physically-reasonable starting values for optimization of the bi-phen linker, with harmonic restraints used as described above.

2.7. *Coordination polymer structure building*

Although a bulk polymer synthesized as described above is likely to be topologically complex, a fairly simple branched polymer topology was chosen in order to facilitate automated structure building. The branched coordination polymer was modeled (figure 2) as a five-generation dendrimer beginning with a single metal center in G_1 (generation 1), which is connected to three metal centers in G_2. These are connected in turn to six metal centers in G_3, 12 in G_4, and 24 in G_5, for a total of 46 metal centers in the five-generation polymer. To build an initial structure, individual bi-phen linker molecules were arranged using an algorithmic procedure. G_1 consists of a single metal center (located at the origin) surrounded by three linkers, placed in the xy-plane at three angular positions: 0, $2\pi/3$, and $4\pi/3$ radians. In G_2, six linkers are added in two pairs; each pair is located at the same angular position as one of the G_1 linkers, at a distance above or below the xy-plane. G_3 adds 12 linkers in two planes above and below the origin, at six equally-spaced angular positions. The process is carried on iteratively, with odd-numbered generations doubling the number of angular positions and even-numbered generations doubling the number of planes (figure 2). The initial layout was designed to avoid steric clashes by placing organic linkers much further apart than they would be in a realistic dendrimer; the optimized MM forcefield was then used to minimize the structure, shortening the unreasonably long metal–nitrogen bonds and arranging the metal ions and organic linkers into a rough starting structure for dynamical simulations.

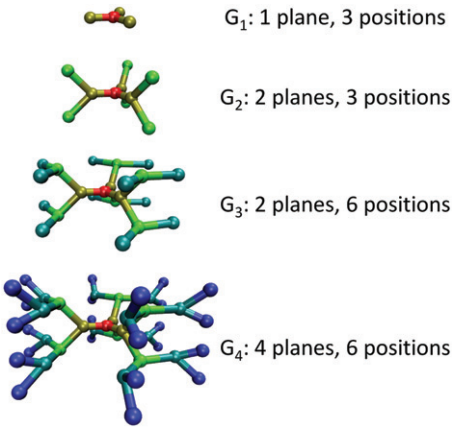

Figure 2. Construction procedure for the coordination dendrimer model. Generation 1 (G_1) consists of a single metal center surrounded by three linkers in a single plane. In each generation, twice the number of linkers is added as in the previous generation; even-numbered generations double the number of planes in which linkers reside, while odd-numbered generations double the number of angular positions within a plane.

A few stereochemical details also needed to be addressed at this stage. CHARMM-type forcefields assign atoms to a limited set of pre-defined types, and only one set of forcefield parameters is permitted for interactions involving a set of atoms of particular types. All the phenanthroline nitrogen atoms were of the same type (since all are chemically identical), but the metal–phenanthroline complexes contain two different types of N–metal–N angles – three 180° angles formed by N atoms on opposite sides of the octahedrally-coordinated metal ion, and twelve 90° angles formed by adjacent pairs of nitrogens. The three 180° angles were omitted from the molecule topology; only distortions of the 90° angles contributed to the energy function. Even if the set of N–metal–N angles to be included in the molecule topology was not correctly identified during the initial structure-building phase described above, the initial minimization step managed to bring incorrectly-assigned metal–nitrogen arrangements into a roughly octahedral geometry, allowing the bond assignments to be corrected in a subsequent step.

In addition, two different types of structural isomerization were possible at each metal center. The metal–phenanthroline complexes are chiral and can assume either a right- or a left-handed geometry. Any enantiomeric excess was corrected by randomly selecting metal centers from the overpopulated stereoisomer, inverting them about their central metal atom, reorienting them to preserve their bonds to the surrounding portions of the polymer, and re-minimizing the entire structure. In addition, the attachment of the thiourea moiety to the phenanthroline ring system is asymmetric. This means that roughly ¼ of the metal centers should have these asymmetric attachment sites in an all-*cis* configuration, while the other ¾ should have one attachment site *trans* to the other two. The initial structure showed an excess of *cis* sites which were corrected by flipping one of the coordinating phenanthroline rings about its C_2 axis, re-assigning the excluded 180° N–metal–N angles as necessary, and re-minimizing the entire molecule.

2.8. *MD calculations*

The optimized coordination polymer forcefield was combined with CHARMM27 parameters for water (TIP3) and chloride ions and simulated using NAMD [26]. Molecular dynamics (MD) simulations used an NpT ensemble with periodic boundary conditions, a Langevin piston for pressure control, and particle mesh Ewald electrostatics. A water box and Cl^- counterions were added using the *solvate* and *ionize* plugins in VMD. Because the initial simulation setup described above is not guaranteed to produce a low-energy conformation, the coordination polymer was subjected to a simulated annealing protocol in which it was heated from 300 to 1000 K in 5 K increments lasting 5 ps each, held at 1000 K for 300 ps, and then cooled back down to 300 K in 5 K increments lasting 50 ps. To avoid a dramatic volume increase with the increasing temperature, simulated annealing used an NVT ensemble with fixed periodic boundary conditions and explicit solvent; this required pre-equilibration of the system at 300 K in an NpT ensemble to obtain the proper volume. During the heating phase, the coordination dendrimer assumed a more extended conformation with a larger radius of gyration; the radius of gyration did not decrease again during the cooling phase, suggesting that the more extended configuration is the physically-realistic conformation for the fully-solvated polymer.

In order to closely approximate the conditions measured in the PDF experiments, the system was subjected to a "simulated drying" protocol. After 5 ns of constant-pressure simulation at 300 K, 50% of the water molecules in the system were removed. When the simulation was re-started with the same boundary conditions, the volume rapidly decreased and the polymer assumed a somewhat more compact conformation. The process was repeated nine times until only 35 water molecules remained (~0.76 H_2O/Fe). In the final phase (figure 3), the remaining water molecules were removed and the system was slowly cooled from 300 K to 5 K in 5 K increments lasting 50 ps each and then optimized using conjugate gradient minimization. To generate desolvated structural models for the Co^{2+}, Ni^{2+}, and Zn^{2+} polymers, the Fe structure with 0.76 H_2O/Fe was used as a starting configuration, metal ions were replaced, and the system was equilibrated at 300 K for 5 ns, after which the same cooling and minimization protocol was applied.

3. Results

3.1. *Experimentally-determined PDFs*

The experimentally-determined radial PDFs $G(r)$ are shown in figure 4, along with model fits. A few features are immediately apparent. One is that the experimental and model curves agree fairly well at low r values, where a few pronounced peaks are characteristic of the coordination polymer structure. At high values of r, however, some samples (particularly the Fe and Ni polymers and the metal-free linker) exhibit low-amplitude peaks that are suggestive of a crystalline contaminant. In the case of metal-free linker and the Ni^{2+} polymer, the contaminant appears to be NaCl, which could have been formed during the ligand synthesis and carried through to the polymers. In the Fe^{2+} sample the high-r peaks were fit well by NH_4Cl, with the ammonium coming from $(NH_4)_2Fe(SO_4)_2 \cdot 6H_2O$ and the Cl^- appearing as carryover from the

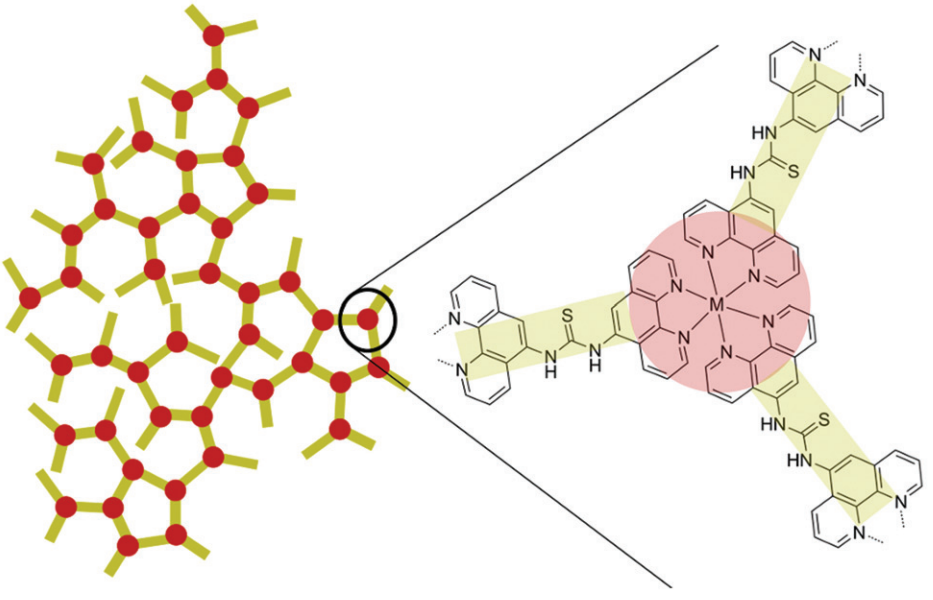

Figure 3. Schematic structure of the metal–organic coordination polymer. Metal sites form trivalent nodes to which three bivalent organic linkers can attach.

ligand synthesis. The polymer structures obtained by simulated lyophilization were used to calculate model PDFs using PDFgui. Three parameters were used in fitting – an overall scale factor, a uniform temperature factor used for all atoms, and an isotropic scaling of the unit cell vectors. For the metal-free, Ni^{2+}, and Fe^{2+} samples, a two-component fit was used, in which the experimental PDF was fit to a linear combination of the simulated polymer PDF and a PDF calculated from the bulk NaCl or NH_4Cl crystal structure. These two-phase fits therefore used a total of six parameters: the original three for the polymer phase, along with a scale factor and temperature factors for the heavy atoms of the contaminant.

3.2. *Refined parameter values*

Refined forcefield parameters were determined for the metal–organic coordination polymer, as described in section 2. Most of the refined forcefield parameters (i.e., bond, angle, and dihedral spring constants) were similar to analogous values in the CHARMM27 forcefield for proteins, particularly those for aromatic rings containing carbon and nitrogen. The nitrogen–metal interactions, however, do not have clear analogues in the protein forcefield, with the exception of Fe–N interactions – the CHARMM27 forcefield contains parameters for heme with a histidine ligand, so parameters for N–Fe bonds both within the heme macrocycle and for the imidazole–Fe ligation are present. These two bonds are modeled rather differently – the heme–Fe bond has a spring constant of 270.2 kcal mol^{-1} $Å^{-2}$, while the histidine–Fe bond has a spring constant of 65.0 kcal mol^{-1} $Å^{-2}$. The values shown in table 1 clearly indicate that the metal–phenanthroline interactions are more similar to the histidine–Fe bond than to

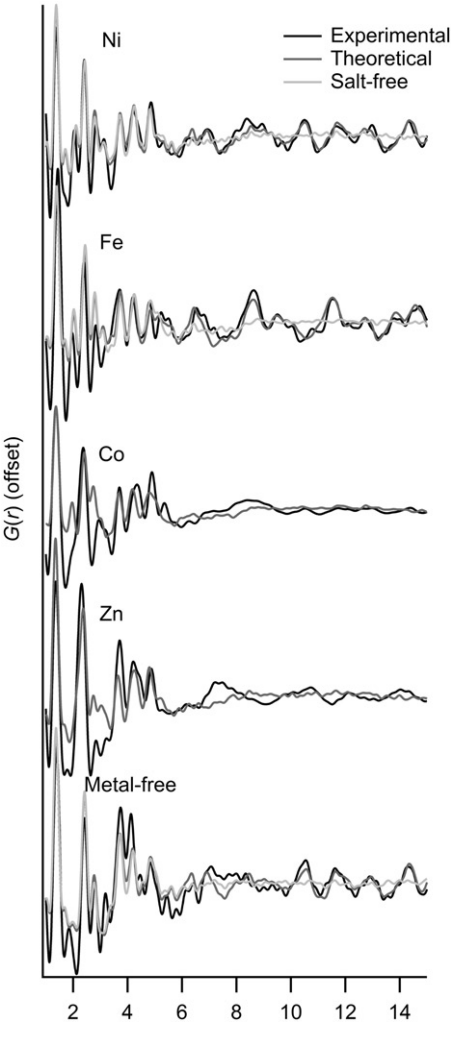

Figure 4. Experimental and fitted PDFs for coordination polymer materials. In some cases (Ni, Fe, metal-free), a contaminating salt phase was introduced in order to provide an adequate fit to the high-*r* region.

Table 1. Refined forcefield parameters for metal–N interactions – the equilibrium distance (b_0) and spring constant (k_b) of the N–metal bond and the bending spring constant (k_θ) for the 90° N–metal–N interaction.

Metal	N–M (b_0)	N–M (k_b)	N–M–N (k_θ)
Co	1.970	69.59	84.23
Fe	2.032	70.80	24.27
Ru	2.125	66.84	35.07
Ni	2.148	39.34	8.32
Zn	2.244	22.22	6.81

Note that the shortest bonds are also the stiffest, with high stretching and bending spring constants. M = metal.

the heme–Fe bond. One clear trend is that metals with a shorter metal–nitrogen bond refine to a much larger spring constant – shorter bonds are stiffer. A similar trend is present for the N–metal–N angle term. The Co–N bonds are short and stiff, and the N–Co–N angle term is also rather stiff, while the longer, more elastic Ni–N and Zn–N bonds correspond to much lower N–Ni–N and N–Zn–N angle spring constants.

3.3. *MD simulation results*

One quantitative way to characterize the conformation of the metal–organic coordination polymer is to look at the geometry about each thiourea linker. Figure 1 shows that the low-energy conformations of this linker can be separated into three categories – an extended conformation (figure 1b) in which the two phenanthroline rings are well-separated and the two thiourea hydrogen atoms face each other, a *trans* conformation (figure 1d) in which one thiourea hydrogen is directed inward and one outward, and a contracted conformation (figure 1c) in which the two phenanthroline ring systems are close together while the thiourea hydrogens point outward. In the gas-phase DFT calculations, the *trans* conformations have the lowest total energy while the extended conformations have the highest energy, due to electrostatic repulsion between the two thiourea hydrogen atoms. In the solvated coordination polymer, the energetic picture will be complicated substantially by solvation and steric frustration, but the thiourea linkers still tend to fall into one of these configurations, distinguishable by the distance between thiourea hydrogen atoms (figure 5a). As the H_2O/metal ratio is decreased during simulated desolvation, the relative populations in these three conformational states undergo a dramatic change (figure 5b). While the fraction of thiourea linkers in the contracted conformation stays roughly constant, the fraction in the *trans* conformation undergoes a steady increase, while the extended conformation decreases. Most of the contracted-conformation linkers are at the periphery of the branched coordination polymer and only coordinate a metal ion at one end. They adopt this conformation in order to facilitate hydrophobic interactions between the two phenanthroline rings attached to the terminal linker; this contracted conformation is sterically unfavorable for linkers coordinating two metal ions. The predominant mode of volume contraction during simulated desolvation is therefore the conversion of extended to *trans*-conformations, with a corresponding decrease in metal–metal distances.

Figure 6(a) shows the average Fe–Fe neighbor distance for each step in the simulated lyophilization. The separations were found by identifying, for each Fe, the shortest distance to another Fe for each frame in the MD trajectory and taking the mean. In the fully-solvated polymer, the distance is about 14 Å, decreasing to about 9 Å as the polymer is dehydrated. For a nearest-neighbor distance of d, the most dense possible arrangement of metal centers would be a hexagonal close packing, in which the distance to second-nearest neighbors is $\frac{2\sqrt{6}}{3}d \approx 1.633d$, twice the height of a regular tetrahedron. In figure 6(b), all metal centers within $1.317d$ (the average of the first and second coordination shell distances) are considered to be part of this first coordination shell. For the fully-solvated polymer, the average number of nearest neighbors is about three, consistent with the branching topology of the coordination polymer. As the polymer is desolvated, metal centers that are not directly bonded come into closer proximity, and the number of nearest neighbors increases to about 4.5, including interactions across the

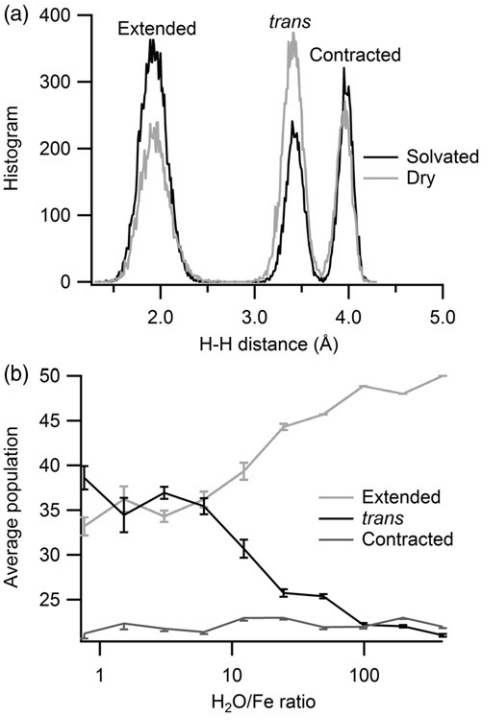

Figure 5. (a) Histogram of distances between the two thiourea hydrogens of the organic linker, showing three distinct populations. The short, medium, and long-distance populations correspond to the extended, *trans*, and contracted conformations in figure 1. (b) Changes in the relative populations of these three conformational states during simulated drying. Most of the contracted population consists of linkers that are at the periphery of the coordination polymer and only coordinate a metal ion at one end; linkers that connect two metal centers usually adopt either the extended or *trans* conformation. As the solvation of the system decreases and the material contracts, the population of linkers coordinating two metal centers shifts from the extended to the *trans* conformation.

periodic boundary conditions. This is still highly inefficient packing, suggesting that the constraints imposed by the thiourea linkages and the volume occupied by the non-chelating phenanthroline rings at the branched polymer periphery interfere significantly with close packing.

Dynamic calculations of H_2O and Cl^- diffusion can also provide invaluable information about coordination polymer solvation as a function of the H_2O/Fe ratio. By comparing the position of a single molecule in different frames of the MD trajectory, the average squared displacement $\langle r^2 \rangle$ was calculated as a function of time. For isotropic 3-D diffusion, this is related to the diffusion coefficient D by $\langle r^2 \rangle = 6Dt$. For the fully-solvated polymer, the diffusion constant of water approaches the standard value of $2.2\,\mu m^2\,ms^{-1}$ and decreases dramatically as water molecules become trapped by the dehydrating polymer. The diffusion coefficients for water and Cl^- follow very similar power-law scaling with the H_2O : Fe ratio (figure 7). The slightly steeper decrease in the Cl^- diffusion suggests that Cl^- interacts with the charged polymer slightly more strongly than does H_2O, restricting the motion of Cl^- at high polymer concentrations.

For many applications it is helpful to know the average metal density, so that the number of metal centers contained in a material segment of a certain size can

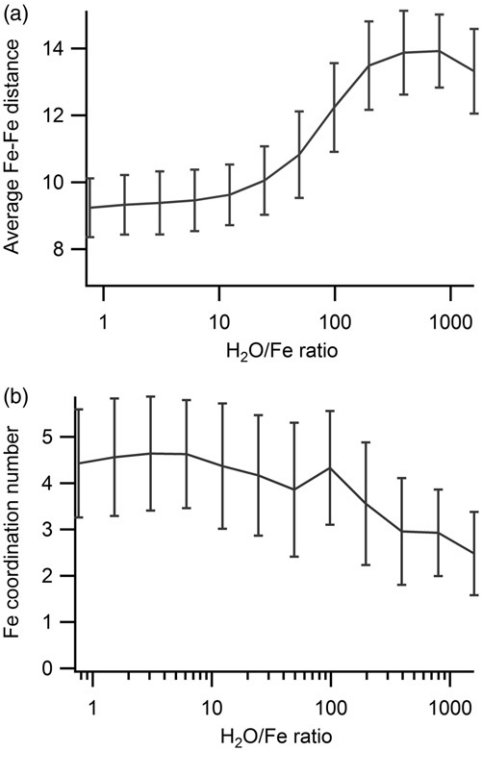

Figure 6. (a) Changes in the metal–metal neighbor distance as a function of simulated drying. The distances shown are the mean of the shortest Fe–Fe distance for each metal center in the simulation. (b) Changes in the average number of nearest neighbors; i.e., the number of metal centers that can be found at a distance close to that shown in (a). At high solvation, this number will be <3 (interior metal centers have a coordination of 3 while surface sites have a coordination of 2), while metal centers in the dehydrated state are often located close to centers other than those to which they are directly linked, resulting in a larger number of nearest neighbors.

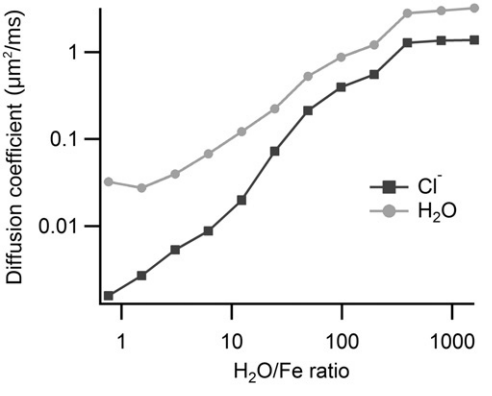

Figure 7. Diffusion of H_2O molecules and Cl^- ions at different levels of desolvation. Both follow a roughly power-law scaling; note that the slope of the decrease in Cl^- diffusion constant is somewhat steeper. This may indicate that, although interactions between the Cl^- ions and the positively-charged polymer are fairly weak and transient, these interactions are somewhat stronger than the H_2O-polymer interactions, leading to a faster decrease in mobility as the solvent volume fraction decreases.

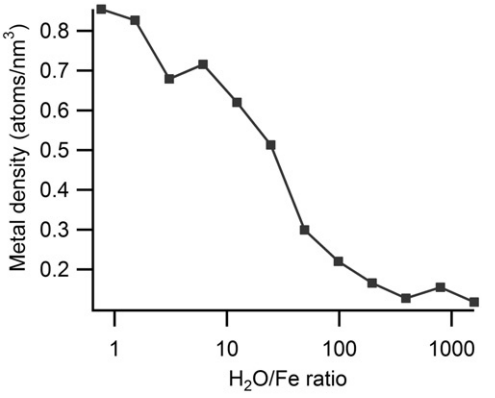

Figure 8. Density of metals near the polymer center; this can be used to estimate the size of the metal–organic coordination polymer that could be synthesized in a constrained environment.

be estimated. If one assumes that the coordination polymer incorporates roughly stoichiometric amounts of metal ions and organic linkers, then its mean density should be similar to what is observed near the interior of a metal–organic dendrimer, before edge effects begin to play a significant role. If this mean density is ρ metal atoms Å^{-3}, then a sphere of radius r around the center of the metal–organic coordination polymer would contain (on average) $\frac{4\pi}{3}r^3\rho$ metal centers. If the observed number of metal centers in such spheres is plotted against r^3, a linear fit can be used to determine the mean density at the center of the coordination polymer. Based on such estimates, the dehydrated coordination polymer has a mean density of 0.85 metal nm^{-3}, while the fully-hydrated polymer yields 0.11 metal nm^{-3} (figure 8).

4. Discussion

The agreement between the experimental and model PDFs shown in figure 4 is rather good and the positions and amplitudes of most peaks in the PDFs are roughly correct. It should be emphasized that no information from the PDF experiments was used in the generation of the polymer structural model – the only specific information used was the structure of bi-phen. One thing that is immediately apparent, however, especially in the samples (Co^{2+} and Zn^{2+}) which did not show significant salt contamination, is that the calculated PDFs are largely featureless beyond about 5 Å. This does not even extend as far as the shortest Fe–Fe distances observed in figure 6, suggesting that the only atom–atom distances that make significant contributions to the PDF are the conformation-independent distances within a single rigid metal–phenanthroline unit. This is not surprising, given the relative lack of order beyond this length scale, and is probably a feature of many poorly-ordered coordination polymer materials.

A few other more subtle features of the PDF analysis also deserve mention. Calculation of a theoretical PDF typically begins with a bulk crystal structure determined by X-ray crystallography. In the absence of thermal disorder, this would produce a PDF with infinitely sharp peaks. In practice, disorder is accounted for by

convolution with atomic thermal factors which tend to shorten and broaden the peaks in the PDF. In the calculations based on the model polymer structures, however, another source of disorder is present – because the structural model is derived from a molecular dynamics simulation, some bond lengths and angles are inevitably non-ideal. Any thermal broadening introduced in the PDF fitting process will result in a further broadening of the PDF peaks beyond what is already introduced by the static disorder in the structural model. For this reason, refinement of the PDF model produced unusually low atomic thermal factors for the polymer phase, because little additional broadening was required to account for the PDF peak width.

In addition, the dimensions of the cubic unit cell were allowed to vary during PDF refinement. For each data set examined, the unit cell dimension decreased by about 2% during refinement, after which the agreement of the model PDF with the low-*r* experimental peaks improved visibly. The equilibrium bond lengths used in the MD forcefield are ultimately based on the optimized geometries determined in the DFT calculations. Measurement of the actual bond lengths obtained in the MD results, however, shows that the C–C, C–N, and C–metal bonds within the phenanthroline ring systems are, on average, 1–2% longer than the values obtained from DFT. C–H bonds and bonds within the thiourea linker are much closer to the DFT values; this is probably because they do not form any closed rings and can therefore minimize to an ideal value without competing constraints. Because the low-*r* peaks in the PDF stem primarily from the numerous rigidly-constrained distances within the metal–phenanthroline complex, this systematic deviation is probably sufficient to account for a ~2% overestimation of the unit cell dimensions.

At longer length scales, the only information available comes from the molecular simulations. While the PDF data are only very informative regarding the rigid structural units surrounding the metal centers, the dynamical simulations contain a wealth of information regarding the flexibility and motion of the coordination polymer. One crucial feature of this system that emerges from the simulation results discussed above is the conformational sensitivity to solvation/desolvation. Within a certain range, features such as the distances between metal centers, the motion of water and ions near the polymer, and the typical conformations adopted by the organic linker molecules are sensitive to the polymer's degree of solvation.

The approach outlined here is likely to be broadly applicable to a variety of coordination polymer materials, both ordered and amorphous. Collection of PDF data on coordination polymer materials is straightforward and choosing materials that form well-ordered MOFs may extend the spatial range of useful information obtained from PDF analysis. Alternatively, other methods of structural analysis (such as solid-state NMR) may be able to provide complementary information. At the computational end, the vital components for molecular simulations of coordination polymers are normal mode calculations of sensibly-chosen building blocks, using DFT or other quantum-chemical methods. This study has focused on a particular combination of metal chelator (phenanthroline) and organic linker (thiourea); the parameterization of other chelators and linkers could proceed along similar lines, and such MM forcefield parameters, once obtained, could be combined to generate a combinatorial number of polymeric materials. As coordination polymer materials become increasingly important for technological applications, multiscale simulation methodologies will likely become increasingly important for analysis and design.

Acknowledgments

This research was supported by grants from the U.S. Department of Energy, Office of Basic Energy Sciences, Division of Materials Science and Engineering DE-FG02-07ER46477. X-ray scattering was obtained at beamline 11-ID-B at the Advanced Photon Source (APS), Argonne National Laboratories, with the assistance of Karena Chapman. The APS is supported by the U.S. Department of Energy under Contract No. DE-AC02-06CH11357. J. Lucon was supported in part by a National Science Foundation graduate research fellowship. DFT calculations were performed on the Louisiana Optical Network Initiative (LONI) Queen Bee cluster, and MD simulations used the Texas Advanced Computing Center (TACC) Ranger cluster; both were accessed through the NSF TeraGrid infrastructure.

References

[1] O.M. Yaghi, M. O'Keeffe, N.W. Ockwig, H.K. Chae, M. Eddaoudi, J. Kim. *Nature*, **423**, 705 (2003).
[2] S. Kitagawa, R Matsuda. *Coord. Chem. Rev*., **251**, 2490 (2007).
[3] A.Y. Robin, K.M Fromm. *Coord. Chem., Rev*., **250**, 2127 (2006).
[4] S. Bureekaew, S. Shimomura, S Kitagawa. *Sci. Technol. Adv. Mater*., **9**, 014108 (2008).
[5] M. Burnworth, L. Tang, J.R. Kumpfer, A.J. Duncan, F.L. Beyer, G.L. Fiore, S.J. Rowan, C Weder. *Nature*, **472**, 334 (2011).
[6] J. Lucon, M.J. Abedin, M. Uchida, L. Liepold, C.C. Jolley, M. Young, T Douglas. *Chem. Commun*., **46**, 264 (2010).
[7] C.C. Jolley, M. Uchida, C. Reichhardt, R. Harrington, S. Kang, M.T. Klem, J.B. Parise, D Douglas. *Chem. Mat*., **22**, 4612 (2010).
[8] N.D. McClenaghan, R. Passalacqua, F. Loiseau, S. Campagna, B. Verheyde, A. Hameurlaine, W Dehaen. *J. Am. Chem. Soc*., **125**, 5356 (2003).
[9] S. Campagna, F. Puntoriero, F. Nastasi, G. Bergamini, V Balzani. *Photochem. Photophys. Coordination Compounds I*, **280**, 117 (2007).
[10] R. Wong, S.J Dolman. *J. Org. Chem*., **72**, 3969 (2007).
[11] P. Debye, H Menke. *Phys. Zeitschr*., **31**, 797 (1930).
[12] T. Egami, S.J.L Billinge. *Underneath the Bragg Peaks: Structural Analysis of Complex Materials*, Pergamon, Kiddington, Oxford, UK, Boston (2003).
[13] A.P. Hammersley, S.O. Svensson, M. Hanfland, A.N. Fitch, D Hausermann. *High Pressure Res*., **14**, 235 (1996).
[14] X. Qiu, J.W. Thompson, S.J.L Billinge. *J. Appl. Crystallogr*., **37**, 678 (2004).
[15] M. Valiev, E.J. Bylaska, N. Govind, K. Kowalski, T.P. Straatsma, H.J.J. Van Dam, D. Wang, J. Nieplocha, E. Apra, T.L. Windus, W de Jong. *Comput. Phys. Commun*., **181**, 1477 (2010).
[16] S.H. Vosko, L. Wilk, M Nusair. *Can. J. Phy*., **58**, 1200 (1980).
[17] C.T. Lee, W.T. Yang, R.G Parr. *Phys. Rev. B*, **37**, 785 (1988).
[18] A.D Becke. *J. Chem. Phys*., **98**, 5648 (1993).
[19] P.J. Stephens, F.J. Devlin, C.F. Chabalowski, M.J Frisch. *J. Phys. Chem*., **98**, 11623 (1994).
[20] P.J. Hay, W.R Wadt. *J. Chem. Phys*., **82**, 270 (1985).
[21] P.J. Hay, W.R Wadt. *J. Chem. Phys*., **82**, 299 (1985).
[22] W.R. Wadt, P.J Hay. *J. Chem. Phys*., **82**, 284 (1985).
[23] A.D. MacKerell, D. Bashford, M. Bellott, R.L. Dunbrack, J.D. Evanseck, M.J. Field, S. Fischer, J. Gao, H. Guo, S. Ha, D. Joseph-McCarthy, L. Kuchnir, K. Kuczera, F.T.K. Lau, C. Mattos, S. Michnick, T. Ngo, D.T. Nguyen, B. Prodhom, W.E. Reiher, B. Roux, M. Schlenkrich, J.C. Smith, R. Stote, J. Straub, M. Watanabe, J. Wiorkiewicz-Kuczera, D. Yin, M Karplus. *J. Phys. Chem. B*, **102**, 3586 (1998).
[24] B.R. Brooks, R.E. Bruccoleri, B.D. Olafson, D.J. States, S. Swaminathan, M Karplus. *J. Comp. Chem*., **4**, 187 (1983).
[25] Z. Cournia, A.C. Vaiana, G.M. Ullmann, J.C Smith. *Pure App. Chem*., **76**, 189 (2004).
[26] J.C. Phillips, R. Braun, W. Wang, J. Gumbart, E. Tajkhorshid, E. Villa, C. Chipot, R.D. Skeel, L. Kale, K Schulten. *J. Comp. Chem*., **26**, 1781 (2005).